Supplementary Information to

“An Intensification of Surface Earth’s Energy Imbalance Since the Late 20th Century”

Li X. et al.

This Supplementary Information document includes:

Tables **S1 to S2**

Figures **S1 to S10**

Table S1: Average Radiation Flux Values from 2000 to 2014 (W/m^2)

Energy budget components	CMIP6-BMA	CMIP6-SMA	Wild 2020	Wild 2015,2019	Trenberth 2020	Kato 2018	Stephens 2012*
SW down radiation	185.8±6.2	188.3±6.1	187	185 (180,188)	160	187	192±11
SW up radiation	23.7±3.4	24.0±3.9	24	25 (23,26)	23	23	23±3
LW down radiation	345.5±5.9	343.4±5.9	344	342 (339,347)	333	344	346±9
LW up radiation	401.4±4.6	400.6±4.5	400	398 (395,400)	390	398	398±5
latent heat	85.8±4.9	85.8±4.9	85	82 (72,85)	82	81	88±10
sensible heat	19.6±4.7	19.6±4.7	20	21 (20,25)	20	25	24±7
EEI	0.7±1.0	1.7±1.0	1.1	0.7 (0.5,0.9)	0.9	0.9	0.6±17

*The data from Stephens, et al. is for the years 2000-2010.

Table S2: 34 CMIP6 Models

Model Name	Affiliated Institution	Country/Region	Resolution
ACCESS-CM2	Commonwealth Scientific and Industrial Research Organisation-Australian Research Council Centre of Excellence for Climate System Science	Australia	192 × 144
ACCESS-ESM1-5	Commonwealth Scientific and Industrial Research Organisation-Australian Research Council Centre of Excellence for Climate System Science	Australia	192 × 144
AWI-CM-1-1-MR	Alfred Wegener Institute, Helmholtz Centre for Polar and Marine Research	Germany	384 × 192
BCC-CSM2-MR	Beijing Climate Center, China Meteorological Administration	China	320 × 160
CAMS-CSM1-0	Chinese Academy of Meteorological Sciences	China	288 × 192
CanESM5	Canadian Centre for Climate Modelling and Analysis	Canada	128 × 64
CanESM5-1	Canadian Centre for Climate Modelling and Analysis	Canada	128 × 64
CAS-ESM2-0	Chinese Academy of Sciences	China	320 × 160
CESM2-WACCM	National Center for Atmospheric Research	USA	288 × 192
CIESM	Climate and Earth System Modeling, Tsinghua University	China	288 × 192
CMCC-CM2-SR5	Centro Euro-Mediterraneo per I Cambiamenti Climatici	Italy	288 × 192
CMCC-ESM2	Centro Euro-Mediterraneo per I Cambiamenti Climatici	Italy	288 × 192
EC-Earth3	EC-Earth Consortium	Europe	512 × 256
EC-Earth3-CC	EC-Earth Consortium	Europe	512 × 256
EC-Earth3-Veg	EC-Earth Consortium	Europe	512 × 256
EC-Earth3-Veg-LR	EC-Earth Consortium	Europe	320 × 160
FGOALS-f3-L	Chinese Academy of Sciences	China	180 × 120
FGOALS-g3	Chinese Academy of Sciences	China	360 × 180
FIO-ESM-2-0	First Institute of Oceanography	China	320 × 160
GFDL-CM4	Geophysical Fluid Dynamics Laboratory	USA	360 × 180
GFDL-ESM4	Geophysical Fluid Dynamics Laboratory	USA	144 × 90
IITM-ESM	Indian Institute of Tropical Meteorology	India	192 × 145
INM-CM4-8	Institute for Numerical Mathematics	Russia	180 × 120
INM-CM5-0	Institute for Numerical Mathematics	Russia	180 × 120
IPSL-CM6A-LR	Institut Pierre Simon Laplace	France	144 × 143
KACE-1-0-G	National Institute of Meteorological Sciences	South Korea	192 × 144
MIROC6	Atmosphere and Ocean Research Institute (The University of Tokyo), National Institute for Environmental Studies, and Japan Agency for Marine-Earth Science and Technology	Japan	256 × 128
MPI-ESM1-2-HR	Max Planck Institute for Meteorology	Germany	384 × 192

MPI-ESM1-2-LR	Max Planck Institute for Meteorology	Germany	192 × 96
MRI-ESM2-0	Meteorological Research Institute	Japan	320 × 160
NESM3	Nanjing University of Information Science and Technology	China	320 × 160
NorESM2-LM	Norwegian Climate Centre	Norway	144 × 96
NorESM2-MM	Norwegian Climate Centre	Norway	360 × 180
TaiESM1	Research Center for Environmental Changes, Academia Sinica	Taiwan	288 × 192

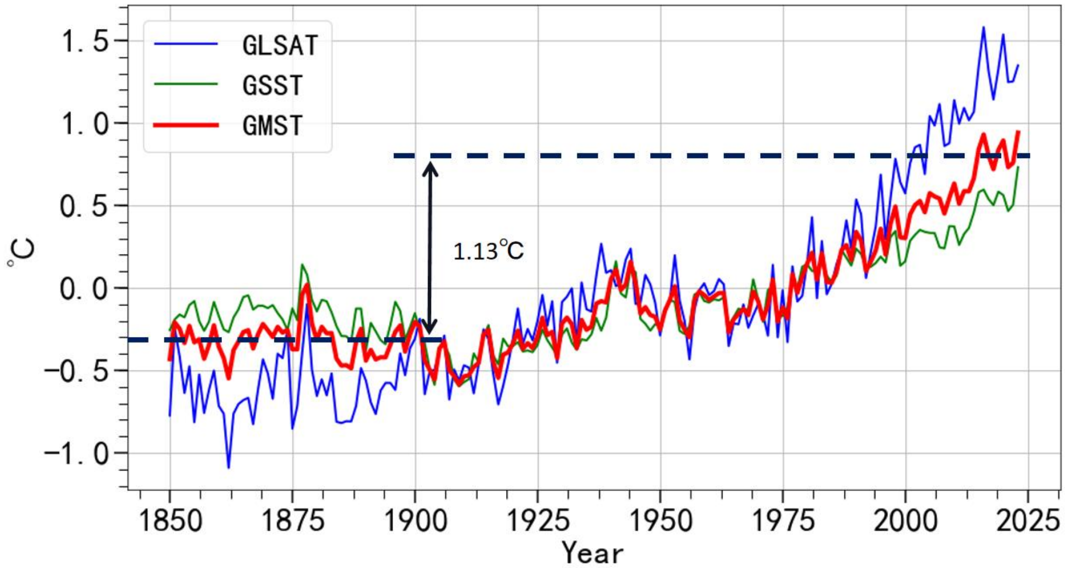

Fi

Figure S1: Time Series of Global Mean Surface Temperature (GMST), Global Sea Surface Temperature (GSST), and Global Land Surface Air Temperature (GLSAT). The dashed lines represent the average levels of GMST for 1850-1900 and for 2014-2023, with a difference of 1.05℃ between the two periods.

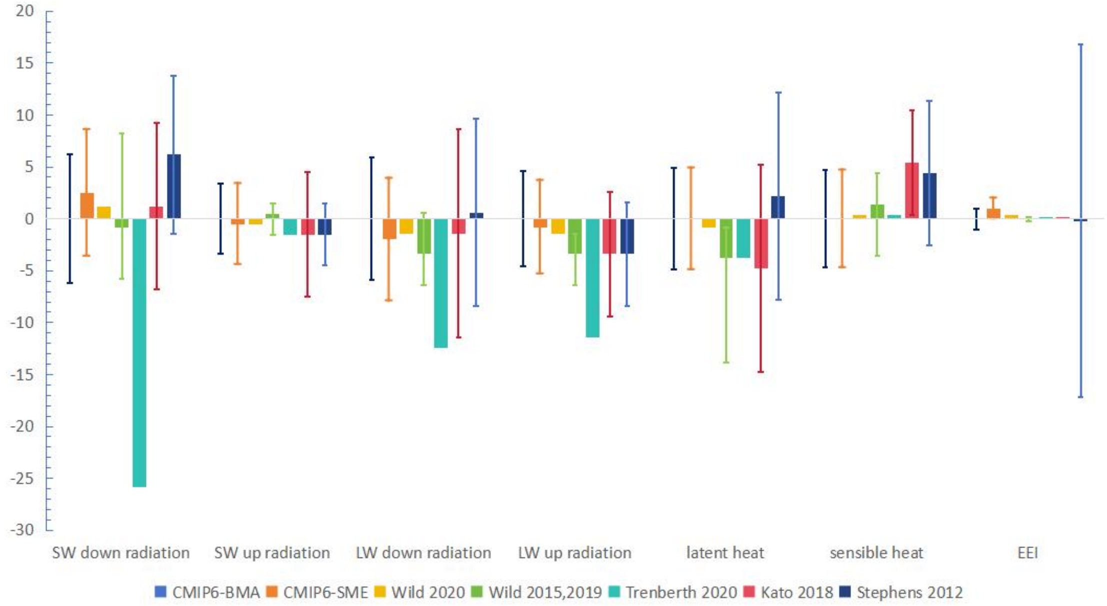

Figure S2: Differences in the radiative components of various budget estimates compared to the BMA results from this study (W/m²). Some components with excessive differences are not shown in the figure; their specific difference values are indicated next to the axes with numbers. Units are in W/m² . The range of uncertainty is indicated by the error bars. Some studies lack a range of uncertainty and only provide the best estimate.

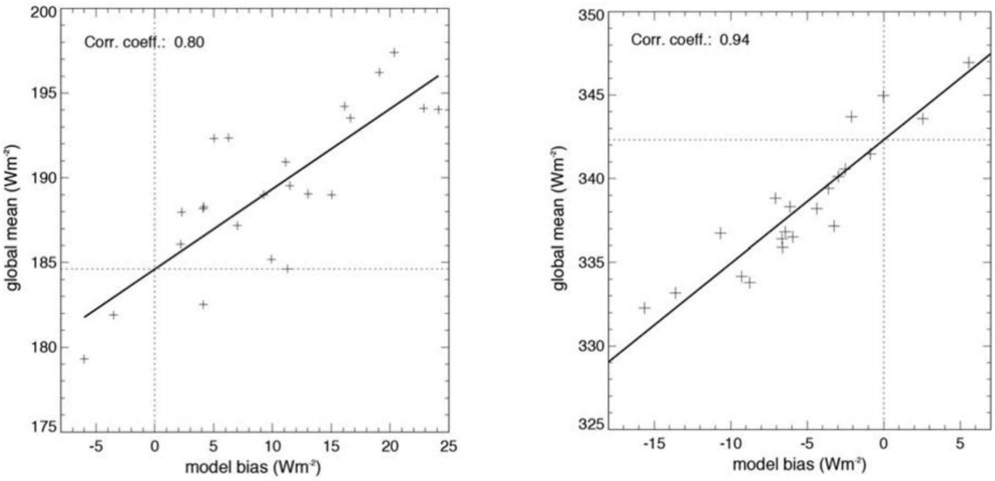

Figure S3: Global mean surface downward shortwave radiation (left) and upward longwave radiation (right) from 22 CMIP5/IPCC AR5 models and ERA40 versus their respective biases averaged over 760 surface observation sites from GEBA. Compared to surface observations, most models overestimate downward shortwave radiation and underestimate upward longwave radiation. The figure is derived from Wild et al. 2013, Figures 12 and 18[1] .

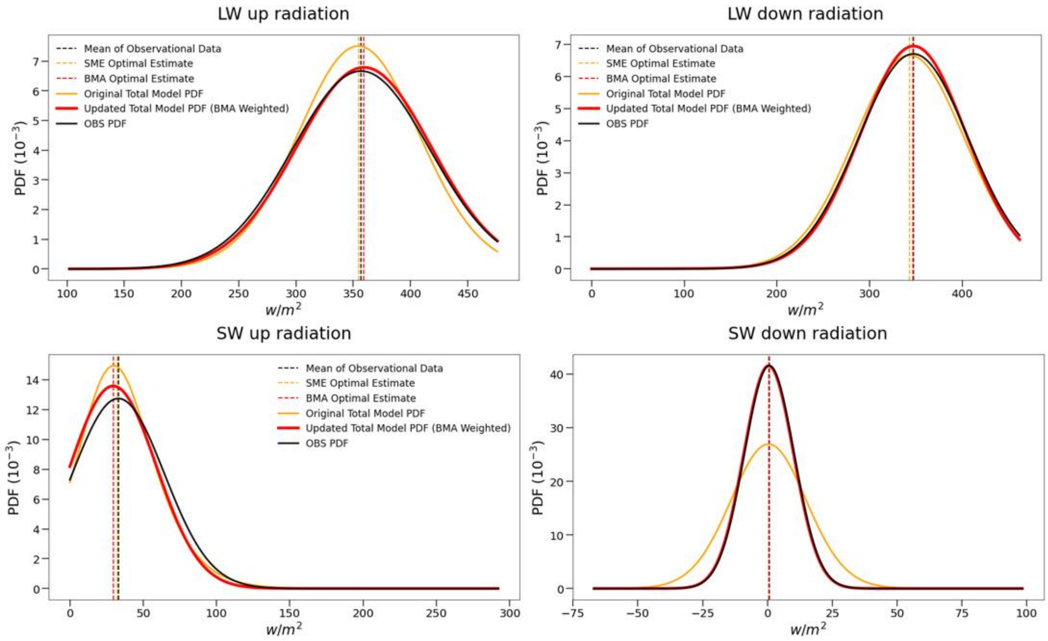

Figure S4: PDF (with ordinate values scaled by a common factor of 10^3) for the SME and BMA results of each radiation component at the grid points corresponding to the observational data. The red line represents the PDF distribution of BMA, the yellow line for the SME's PDF distribution, and the black line for the PDF distribution of observational data. The dashed lines represent the optimal estimate results for each distribution.

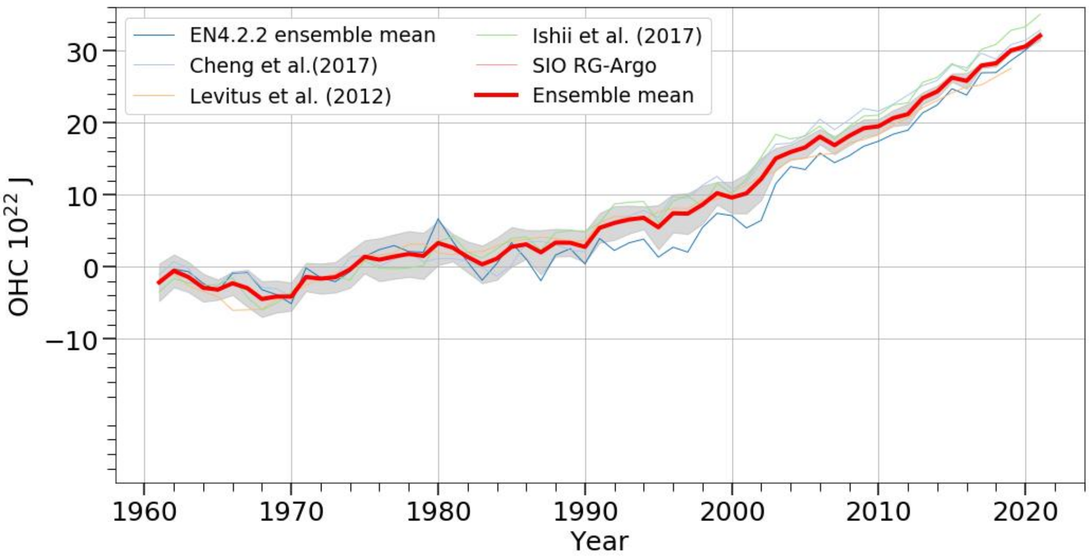

Figure S5: Time Series of Anomalies in Ocean Heat Content (OHC) from 0-2000 meters relative to the 1961-1990 average. Thin lines represent different OHC observational data (Levitus et al. 2012, Cheng et al. 2017, Ishii et al. 2017, Good et al. 2013, Roemmich et al. 2009), with the red line indicating the overall mean OHC. The shaded area shows the uncertainty range drawn using twice the standard deviation.

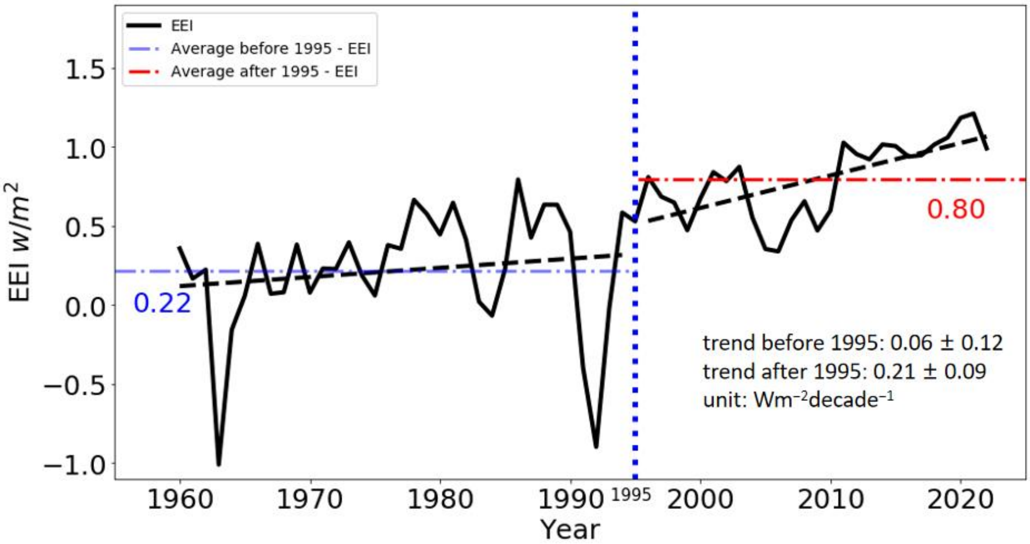

Figure S6: Changes in the average values and trends of EEI before and after 1995, the trend excluding specific years represents the rends before 1995 after excluding extreme values from the volcanic years of Agung (1963), Kilauea in Hawaii (1983), and Pinatubo in Indonesia (1991). The t-test results have a 95% confidence level.

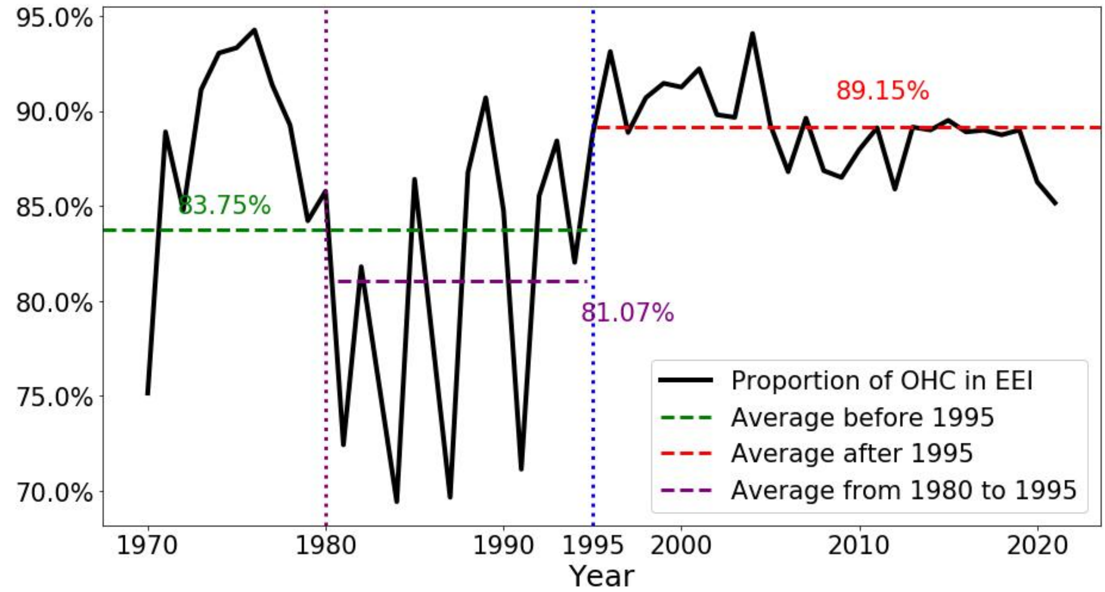

Figure S7: Time series of the proportion of OHC change in EEI and the changes in its average values before and after 1995. The data has been subjected to a 10-year moving average treatment, and the t-test results have a 95% confidence level.

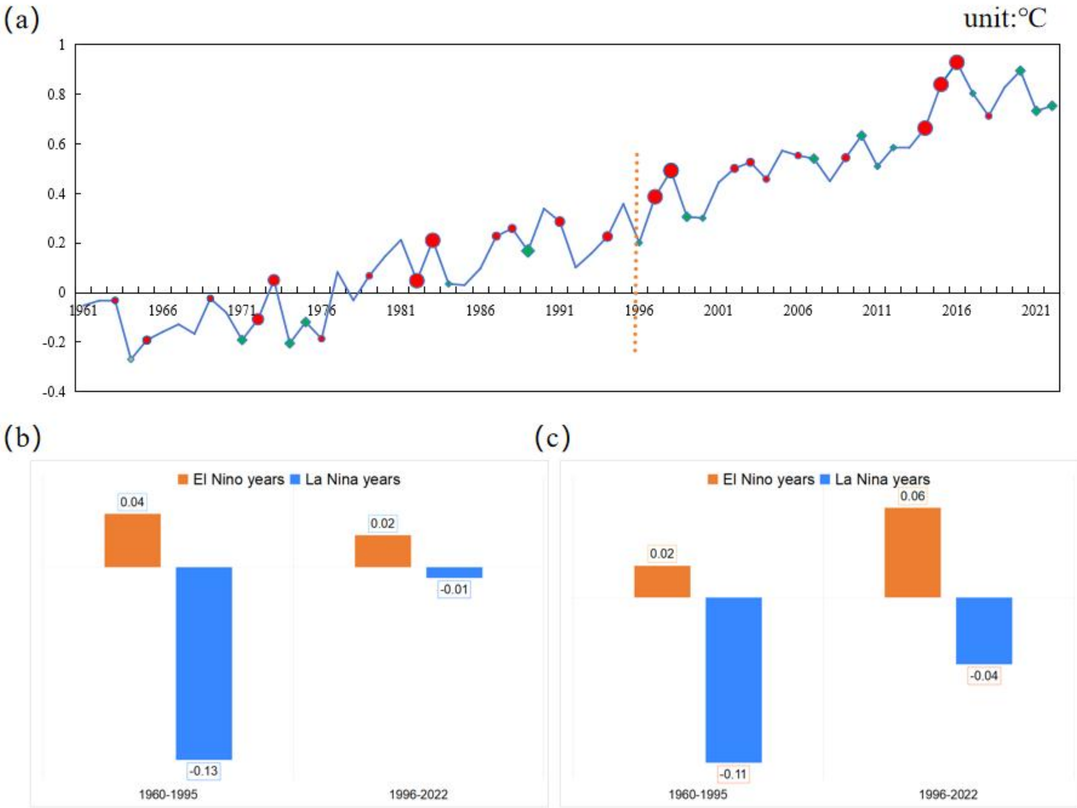

Figure S8: (a) Relationship between the GMST Time Series and ENSO Events. Red circular dots represent El Niño events, with the size of the dots indicating the intensity of the events; larger dots correspond to stronger El Niño events. Green diamond-shaped dots represent La Niña events, with the size of the diamonds indicating the event's intensity; larger diamonds correspond to stronger La Niña events. (b) Anomalies in the average temperatures during El Niño years and La Niña years compared to the overall annual average temperature anomalies. (c) the same as (b), except for the anomalies in the average temperatures has been detrended. In both cases, through T-test, there is a significant difference between the average temperature anomalies of El Niño and La Niña years and the annual average temperature anomalies at a 95% confidence level, respectively.

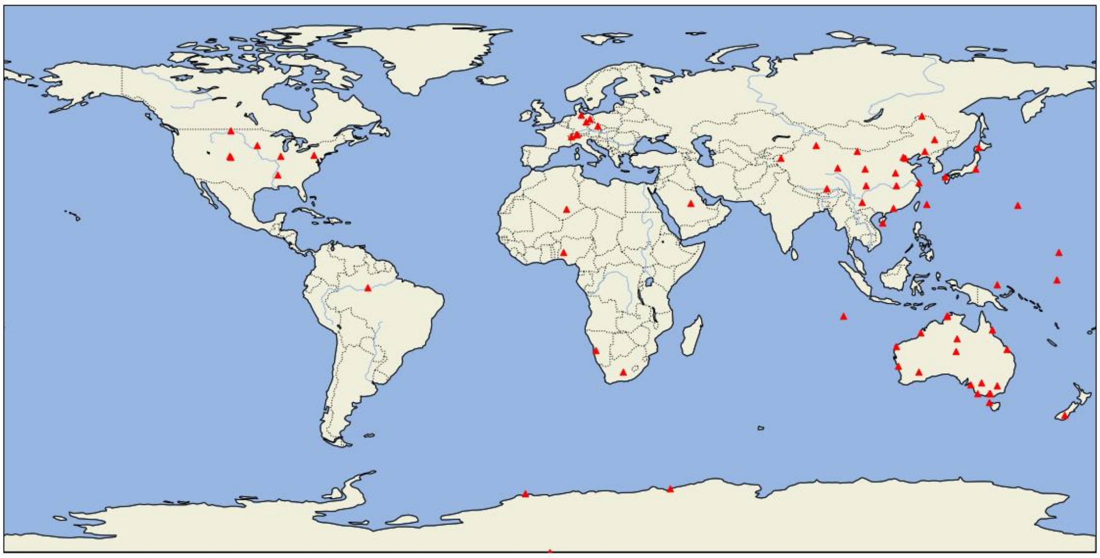

Figure S9: Geographical Distribution of GEBA Observation Sites Used in This Study.

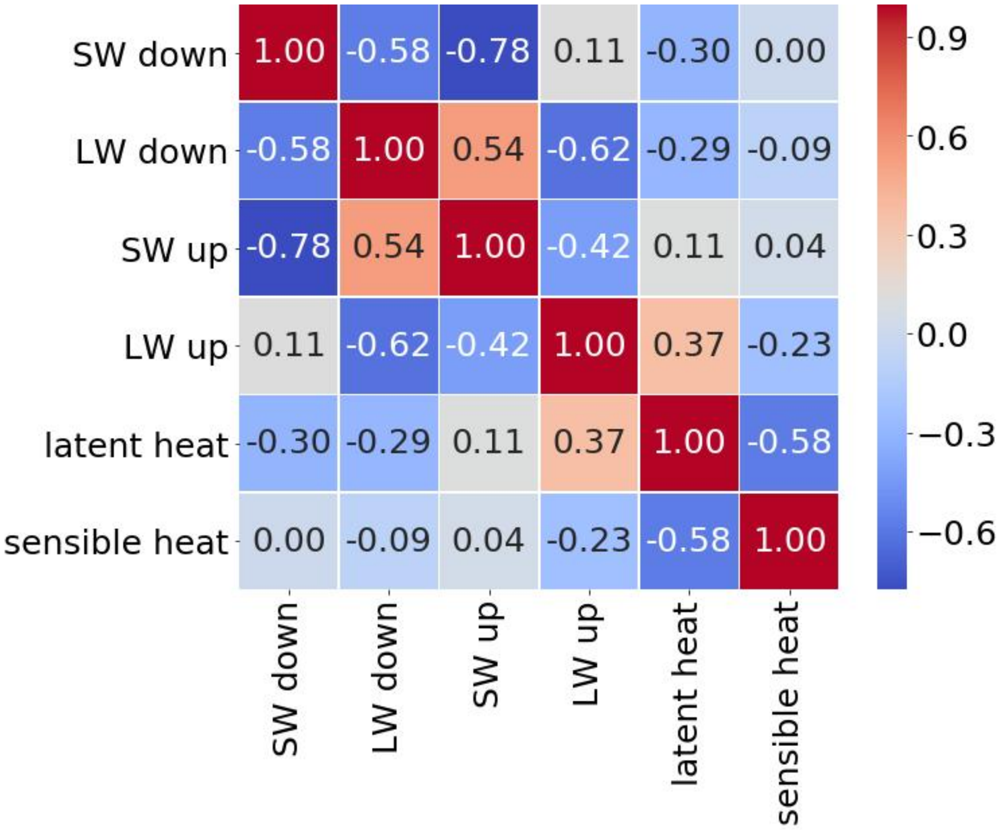

Figure S10: Pearson Correlation Coefficients for Various Radiation Components in 2000.

1. Wild, M., Folini, D., Schär, C., Loeb, N., Dutton, N. E. G., & König-Langlo, G. (2013). The global energy balance from a surface perspective. Climate Dynamics, 40, 3107–3134.